

GAMMA-RAY EMISSION FROM ROTATION-POWERED PULSARS

JOHANN A. HIBSCHMAN

Theoretical Astrophysics Center, Astronomy Department, University of California, Berkeley

601 Campbell Hall, Berkeley, CA 94720-3411

jhibschan@astron.berkeley.edu

Draft version October 23, 2018

ABSTRACT

Using a simplified model of cascade pair creation over pulsar polar caps presented in two previous papers, we investigate the expected gamma-ray output from pulsars' low altitude particle acceleration and pair creation regions. We divide pulsars into several categories, based on which mechanism truncates the particle acceleration off the polar cap, and give estimates for the expected luminosity of each category.

We find that inverse Compton scattering above the pulsar polar cap provides the primary gamma rays which initiate the pair cascades in most pulsars. This reduces the expected γ -ray luminosity below previous estimates which assumed curvature gamma ray emission was the dominant initiator of pair creation in all pulsars. Even for the brightest pulsars where curvature radiation sets the height of the pair formation front (PFF), we find predicted luminosities too low to explain the EGRET pulsars, suggesting that the source of that emission is an outer magnetosphere accelerator. The predicted polar cap luminosities are large enough, however, to be observable by upcoming γ -ray instruments, which provides a firm test for this theory.

Subject headings: Acceleration of particles—gamma rays: theory—pulsars: general

1. INTRODUCTION

Although only a few pulsars have so far been detected in γ -rays, mostly via the EGRET telescope on CGRO (Ulmer 1994; Thompson, et al. 1997), this number should steadily grow as a new generation of γ -ray instruments, such as INTEGRAL and GLAST, is brought online. This should greatly assist theoretical understanding of pulsars, since the highest energy photons provide a direct window into the underlying mechanisms thought to lead to pulsar emission of all types.

The primary photon emission mechanisms important in radio pulsars are inverse Compton scattering (ICS), in both the resonant (RICS) and Klein-Nishina nonresonant (NRICS) modes, and curvature emission. The relative importance of these mechanisms is still unclear. Most γ -ray pulsar papers have concentrated on the curvature emission (Zhang & Harding 2000; Romani & Yadrioglu 1995; Daugherty & Harding 1982), while an increasing number of polar-cap physics papers have emphasized the importance of ICS (Dermer 1990; Sturner 1995; Sturner, et al. 1995; Luo 1996; Harding & Muslimov 1998).

In the polar-cap acceleration model, particles are extracted from the polar cap and accelerated by large rotation-induced electric fields, forming the primary beam. These particles then emit primary γ -ray photons due to ICS and curvature emission, and these photons interact with the pulsar magnetic field to create electron-positron pairs. The density of these secondary pairs increases with height as more and more photons pair-produce, until the pair density is sufficient to short out the accelerating field.

Historically, this shorting of the accelerating field was thought to occur in a thin layer after the creation of the first pair; hence, the region of no pair creation, $E_{\parallel} \neq 0$, was thought to be separated from the region of copious pair creation, $E_{\parallel} \approx 0$, by a thin “pair formation front” (PFF).

ICS photons, however, create small numbers of pairs at low altitudes, breaking the connection between the altitude of the first created pair and the altitude at which the electric field disappears. Since the altitude of the first created pair has no inherent dynamical significance, we use the term PFF in this paper always as applying to the altitude at which the accelerating field is shorted. Other effects, such as the polarization of the generated pairs, will also begin at the point of first pair creation, but these effects must likewise reach some threshold before they affect the dynamics of the beam.

Once the accelerating field has been shorted out, the primary beam coasts, continuing to emit γ -rays. The total γ -ray output of a polar cap is then a combination of the synchrotron γ -rays produced by the created secondary particles, the ICS radiation emitted by the secondary particles, and the primary γ -rays emitted by the primary beam. If the primary beam is radiation-reaction limited, this emission efficiently converts the beam energy into γ -rays; otherwise, only a small fraction is extracted.

We find that the γ -ray output of pulsars falls into two categories. For the majority of pulsars, non-resonant ICS stops the beam acceleration at small Lorentz factors where γ -ray emission is inefficient, leading to low luminosities. For the remaining pulsars, the beam is accelerated to high Lorentz factors, resulting in efficient γ -ray emission, and a high luminosity.

Using the results of Hirschman & Arons (2001a) and Hirschman & Arons (2001b), henceforth Papers I and II, we examine the boundary between these categories of pulsars, and predict the luminosities and spectral characteristics of these objects.

2. MODEL

Inverse Compton scattering depends strongly on the temperature of the neutron star polar cap, making the

thermal cooling model chosen for the neutron star an important part of the theory. For simplicity, we will assume the temperature of the polar cap is entirely due to the polar cap heating discussed in Paper I. We use the acceleration model of Muslimov & Tsygan (1992); Muslimov & Harding (1997), in the simplified form described in Paper I, and neglect spatial variations across the polar cap.

This accelerating potential, expressed in units of mc^2/e so as to give the expected particle Lorentz factor, is

$$\begin{aligned}\Phi_{low}(t) &= \Phi_1 t^2 \quad mc^2 e^{-1}, \quad t < 1 \\ \Phi_{high}(t) &= \Phi_1 t \quad mc^2 e^{-1}, \quad t > 1\end{aligned}\quad (1)$$

where $\Phi_1 = 5.14 \times 10^4 B_{12} P^{-5/2}$, $t \equiv s/s_1$, and $s_1 = 8.87 \times 10^{-3} P^{-1/2} R_*$, while s is the altitude above the stellar surface.

Although we use general relativity though the Muslimov and Tsygan accelerating potential, we neglect other relativistic effects, such as the changes to the magnetic field near the surface and the gravitational red-shift of the emitted photons. These effects are of order 10–15%, so including them would pretend to greater accuracy than justified. The accelerating potential is unique, as it is only the charge difference created by the relativistic contribution which creates the starvation electric field.

2.1. Emission rates

First, we consider the emission of a single primary beam particle, moving along the field lines above the pulsar cap. We neglect, for now, discussion of the secondary particles created by pair-production, as the total energy emitted by these particles is clearly limited by that emitted by the primaries. For this section, we effectively assume that only a negligible fraction of the energy emitted in primary γ -rays remains in the generated electron-positron plasma. From the results of Paper II, this naturally follows in low- B pulsars ($B_{12} \approx 1$) and results in other pulsars due to the RICS of the secondary pair plasma.

Since NRICS is only logarithmically-dependent on the Lorentz factor of the beam, the NRICS power emitted is limited primarily by the attenuation of the background thermal photons as the beam particles move away from the star. If we assume a hot polar cap of angular radius $\theta_c = \sqrt{\Omega R_*}/c$, where Ω is the angular velocity of the pulsar, $\Omega = 2\pi/P$ and R_* is the radius of the neutron star, assumed to be 10 km, the total energy radiated by one particle is

$$E_{NR} = \frac{\theta_c R_*}{c} P_{NR} = 6.1 \times 10^{-4} P^{-1/2} T_6^2 \text{ ergs} \quad (2)$$

The approximate form used for the NRICS power, P_{NR} , is that given in Paper I, and T_6 is the temperature of the polar cap, in units of 10^6 K.

The power emitted via RICS, while only logarithmically sensitive to the decline in the thermal photon flux, decreases quickly with increasing Lorentz factor. Because of this dependence, most of the RICS power is emitted at low altitudes where the Lorentz factor is still small. The expected total output per particle is

$$E_R = \frac{s_{min}}{c} P_R(\gamma_{min}) = 4.5 \times 10^{-5} P^{3/4} B_{12} T_6^{3/2} \text{ ergs} \quad (3)$$

where $\gamma_{min} = \epsilon_B/kT$ is the minimum Lorentz factor at which thermal photons are upscattered into resonance

with the beam, s_{min} is the altitude at which the beam particles reach γ_{min} , and P_R is the power emitted by RICS emission, as given in Paper I. In the acceleration model from Paper I, $s_{min} = 450 P^{3/4} T_6^{-1/2}$ meters, assuming a star of radius 10 km.

The power emitted by curvature radiation is strongly dependent on the Lorentz factor of the beam, varying as γ^4 , so most of the energy emitted by curvature radiation is emitted as the beam coasts above the PFF. Once particle acceleration stops, the Lorentz factor of the primary beam declines according to

$$\gamma(s > s_{PFF}) = \gamma_{PFF} \left(1 + 3 \frac{P_C(\gamma_{PFF})}{\gamma_{PFF}} \frac{R_*}{c} \ln \frac{1+s}{1+s_{PFF}} \right)^{-1/3}, \quad (4)$$

assuming a dipolar magnetic field. The upper limit may be estimated by finding the altitude at which the high-energy primary beam decouples from the magnetic field. Equating the energy density in the beam to the energy density in the magnetic field gives a decoupling height of $r_{max} = 4123 B_{12}^{1/3} P^{1/3} \gamma_7^{-1/3} R_*$, where γ_7 is the Lorentz factor of the beam in units of 10^7 . The PFF is close to the surface, so the logarithm above is approximately 8.3.

The total curvature energy emitted is then

$$E_C = (\gamma_{PFF} - \gamma(s_{max})) mc^2 = 8.2(\gamma_{PFF} - \gamma_7(s_{max})) \text{ ergs.} \quad (5)$$

Comparing the emitted energies, equations (2), (3), and (5), we find that for typical Lorentz factors of $\gamma_{PFF} > 10^5$, only the curvature emission may radiate any appreciable fraction of the beam particle energy. The minimum Lorentz factor at which radiation reaction is important is then

$$\gamma_{RR} = 2.33 \times 10^7 P^{1/3}, \quad (6)$$

which is the Lorentz factor at which the primary beam particles lose half their energy to curvature radiation. Above this Lorentz factor, roughly all of the energy in the beam is lost to γ -rays; below, the beam propagates without significant radiation losses.

The expected curvature energy loss in these two regimes is

$$E_C \approx \gamma_{PFF} mc^2 = 8.2 \times 10^{-7} \gamma_{PFF} \text{ ergs} \quad (7)$$

if radiation reaction is important and

$$E_C \approx \frac{8.3 R_*}{c} P_C(\gamma_{PFF}) = 1.51 \times 10^{-28} P^{-1} \gamma_{PFF}^4 \text{ ergs} \quad (8)$$

if not.

2.2. Luminosity

Using the polar cap model from Paper I, we can classify pulsars according to the mechanism which sets the PFF and whether the beam is radiation reaction limited ($\gamma_{PFF} > \gamma_{RR}$). The pair formation model then gives the altitude of the PFF, s_{PFF} , and the Lorentz factor at that altitude, γ_{PFF} .

Given γ_{PFF} , we can compute the total expected luminosity by multiplying the total energy emitted by a single beam particle by the number of particles emitted by the polar cap, $\dot{N} = n_{GJ} c \theta_c R_*^2 = 1.37 \times 10^{30} B_{12} P^{-2} s^{-1}$, where n_{GJ} is the expected Goldreich-Julian number density, $n_{GJ} = \Omega \cdot B / 2\pi c e$.

As a slight modification to the model in Paper I, we find that, in comparison with the numerical results of Paper II, the PFF from curvature emission is more accurately found by finding the altitude at which the first pair is formed. This is due to the steadily increasing intensity of curvature emission with increasing Lorentz factor.

A curvature photon emitted at altitude s will pair produce at

$$s_{\pm} = s + \frac{1}{4} \frac{\epsilon_a}{\epsilon_C(\gamma(s))} R_*, \quad (9)$$

where ϵ_C is the typical curvature photon energy, $\epsilon_C = 5.8 \times 10^{-19} \gamma^3 \rho_8^{-1} mc^2$, and ϵ_a is the scaling energy for pair production from Paper I, $\epsilon_a = 2166 B_{12}^{-1} P^{1/2} f_\rho$. Here f_ρ is the ratio of the actual field line radius of curvature to the radius of curvature of the dipole field line which intersects the stellar surface at θ_c ; for the remainder of the paper, this is taken to be 1.

The minimum value of this is at

$$s_{PFF,C} = 1.91 B_{12}^{-1} P^{7/4} f_\rho^{1/2} R_*, \quad (10)$$

if the PFF takes place in the linear regime of the accelerating potential at $s \gtrsim \theta_c R_*$, or

$$s_{PFF,C} = 0.211 B_{12}^{-4/7} P^{11/14} f_\rho^{2/7} R_*, \quad (11)$$

if in the quadratic regime at $s \lesssim \theta_c R_*$.

Using the semi-numerical model of Paper II, we then classify pulsars by which the emission mechanism produced the PFF, by whether the PFF occurred at low or high altitude (in comparison with the polar cap width), and by whether the beam was radiation-reaction limited. In principle, this gives 12 categories; in practice, there are only five important divisions.

Out of the 540 pulsars in the Princeton pulsar catalog with positive \dot{P} , the majority, 315, had a PFF set by NRICS at high altitude with $\gamma_{PFF} < \gamma_{RR}$. For all of these objects, curvature radiation is the primary energy loss mechanism in the beam drift region above the PFF. Although most of the radiated energy is curvature emission, it is the relatively sparse, but individually much higher-energy, NRICS photons that first pair produce and set the PFF.

In the model of Paper I, self-consistent cap heating produces a PFF height and final Lorentz factor of

$$s_{PFF,NR,pc} = 0.749 B_{12}^{-4/3} P^{11/6} R_* \quad (12)$$

$$\gamma_{PFF,NR,pc} = 4.34 \times 10^6 B_{12}^{-1/3} P^{-1/6} \quad (13)$$

which corresponds, through equation (8) to a total luminosity of

$$L_{NR} = 7.3 \times 10^{28} B_{12}^{-1/3} P^{-11/3} \text{ erg s}^{-1}. \quad (14)$$

This is much lower than previous estimates of pulsar γ -ray luminosity, and is by far the most common case. However, this estimate is only strictly accurate for magnetic fields less than or on the order of 10^{12} Gauss due to the increasing fraction of particle energy left in the particles at higher values of B , as discussed in Paper II. For higher fields, the luminosity will be larger, as NRICS is less efficient, but still less than the value expected from pure curvature radiation.

The next most common case is high-altitude inertially limited RICS, accounting for 126 of the 540 pulsars. For most of these pulsars, the γ -ray emission in the beam drift

region above the PFF is again dominated by curvature emission; the 23 of these where this is not true are among the least luminous pulsars, and so we neglect them.

From Paper I, the PFF height and final Lorentz factor in this case are

$$s_{PFF,R,pc} = 9.66 B_{12}^{-16/7} P^{1/2} R_* \quad (15)$$

$$\gamma_{PFF,R,pc} = 5.60 \times 10^7 B_{12}^{-9/7} P^{-3/2} \quad (16)$$

which corresponds, via equation (8), to a total luminosity of

$$L_R^{high} = 2.0 \times 10^{33} B_{12}^{-29/7} P^{-9} \text{ ergs s}^{-1}. \quad (17)$$

The third category combines those pulsars where either curvature or NRICS sets the PFF at high altitude and where the beam is radiation reaction limited, for a total of 57 objects. In practice, we find that these pulsars are all well-modeled by the expected PFF for curvature emission, equation (10), and equation (7) for the energy loss. This gives a final Lorentz factor and total luminosity of

$$\gamma_{PFF,C}^{high} = 1.10 \times 10^7 P^{-1/4} \quad (18)$$

$$L_C^{high} = 1.2 \times 10^{31} B_{12} P^{-9/4} \text{ ergs s}^{-1} \quad (19)$$

which is essentially the same as the Zhang & Harding (2000) value for their regime II. As they mentioned, this preserves the empirical $L_\gamma \propto L_{SD}^{1/2}$ relation. These are among the brightest γ -ray pulsars, behind only category 4 in total luminosity.

The fourth category is similar to the third, in that it includes radiation reaction limited beams where the PFF is set by both curvature and NRICS emission, but at low altitudes rather than high. These are the 21 brightest, highest-potential pulsars. Using equations (11) and (7) gives a Lorentz factor and luminosity of

$$\gamma_{PFF,C}^{low} = 2.90 \times 10^7 B_{12}^{-1/7} P^{1/14} \quad (20)$$

$$L_C^{low} = 3.3 \times 10^{31} B_{12}^{6/7} P^{-27/14} \text{ ergs s}^{-1} \quad (21)$$

which corresponds to regime I of Zhang & Harding (2000).

The final category consists of the 13 pulsars where RICS sets the PFF in the low-altitude regime, with an inertially limited beam. These are all pulsars with fields well in excess of 10^{13} Gauss, field strengths beyond the expected range of validity of this theory. The the low-altitude PFF height and Lorentz factor are

$$s_{PFF,R,pc}^{low} = 4.03 B_{12}^{-2} P^{3/8} R_* \quad (22)$$

$$\gamma_{PFF,R,pc}^{low} = 1.06 \times 10^{10} B_{12}^{-3} P^{-3/4}. \quad (23)$$

For these pulsars, RICS emission produced more gamma-rays than curvature, so using the emitted energy from equation (3), we find a luminosity of

$$L_R^{low} = 7.2 \times 10^{26} B_{12}^{5/4} P^{-67/32} \text{ ergs s}^{-1}. \quad (24)$$

As in Paper I, the emission mechanism with the smallest PFF height is the dominant mechanism. Owing to the multiplicity of categories, generalizations are difficult, but we can derive a few formulae for the boundaries between regimes by considering only the high-altitude limits.

In this simplest approximation, the boundary between the NRICS-dominated and curvature-dominated pulsars is at $B_{12} = 0.061 P^{1/4}$. Pulsars with weaker magnetic fields are dominated by curvature, and equation (19) is the appropriate luminosity, while pulsars with fields stronger

than this are dominated by NRICS and equation (14) is appropriate. However, this ignores the weakening of NRICS with increasing magnetic field discussed in Paper II, and so should be taken as a statement that the millisecond pulsars are certainly controlled by curvature, while the higher-field, longer-period pulsars are favored by NRICS, but must be examined carefully, using either the full algebraic results from Paper I or the semi-numerical model of Paper II.

The boundary between NRICS and RICS lies at $P_{NR,R} = 6.81 B_{12}^{-5/7}$, with higher periods favoring RICS, while that between RICS and curvature is at $P_{R,C} = 3.66 B_{12}^{-36/35}$, again with RICS dominating at longer period. For pulsars with magnetic fields larger than approximately 4×10^{12} Gauss, NRICS is ineffective in setting the PFF, and the only active mechanisms are RICS and Curvature; at mid-range fields between 3×10^{11} Gauss and 4×10^{12} Gauss, NRICS sets the PFF, while at lower fields, curvature sets it.

2.3. Flux

Since in this model the observed γ -rays originate from particles moving along the field lines above the pulsar polar cap, the predicted luminosities translate directly into a predicted flux. Since the polar cap is the source of the γ -rays, they are beamed into a cone of opening angle $\theta \approx (3/2)\theta_c$. In general, this opening angle will vary with the altitude of the emission, but for most pulsars the altitude of the PFF is small compared to the stellar radius, so simply evaluating the opening angle at the surface is sufficient. If the luminosity is spread evenly throughout this cone, this produces a peak flux of

$$\phi_{peak} = \frac{L}{\pi\theta^2 d^2} \quad (25)$$

where d is the distance to the pulsar. This is the flux seen while looking “down the barrel of the gun.” Only if the spin axis of the pulsar is nearly aligned with the line of sight will the observed flux be on this order. The average flux is reduced by θ/π if the spin axis is perpendicular to the line of sight and by approximately $\theta/\pi \sin \alpha$ in the general case, where α is the angle between the magnetic moment and the rotation axis and we have effectively assumed that the observer’s line of sight passes through the center of the emitting cone ($\beta = 0$). This represents the fraction of the pulse period where the emitting cone is directed towards the observer.

$$\phi_{ave} = \frac{L}{2\pi^2 \theta \sin \alpha d^2}. \quad (26)$$

This average flux is the observable, not the total luminosity. In terms of the luminosities from the previous section, this flux is

$$\phi_{ave} = 3.7 \times 10^{-43} P^{1/2} (\sin \alpha)^{-1} d_{kpc}^{-2} L \text{ ergs cm}^{-2} \text{ s}^{-1}. \quad (27)$$

Since the $\sin \alpha$ term is a factor of order unity, and these approximations are only good to approximately a factor of 2, we simply set it to 1 for the remainder of the paper. We plot the expected observable flux as a function of the pulsar period using a fiducial pulsar distance of 1 kpc in Figure 1, to show the inherent dependencies on pulsar parameters, and using the estimated distances of each individual object in Figure 2, to show the predicted observable flux.

3. SPECTRAL SHAPE

In the previous section, we discussed the total energy output of the pulsar; here, we turn to the expected shape of the spectrum itself. In Paper II, we found that a cascade of pair creation from a single absorbed photon produces a response with a power law index of $-3/2$, due to the reprocessing of synchrotron photons. In order to be absorbed, however, the photon must have an energy greater than $\epsilon_{min} = 5134 B_{12}^{-1} P^{1/2} mc^2$, presuming that the photon was emitted parallel to the magnetic field at the edge of the polar cap at the surface of the star.

Since most of the power emitted in γ -rays from pulsar polar caps is due to curvature emission, except for the few extreme high-field objects where RICS dominates, the energetics of the curvature photons determine the shape of the spectrum. The minimum Lorentz factor for curvature pair production may be found by equating $\epsilon_C(\gamma) = \epsilon_{min}$, yielding

$$\gamma_C = 2.01 \times 10^7 B_{12}^{-1/3} P^{1/3} \quad (28)$$

which is the Lorentz factor at which the critical curvature energy $\epsilon_C(\gamma) = 5.8 \times 10^{-19} \rho_8^{-1} \gamma^3 mc^2$ equals the minimum energy to pair produce, ϵ_{min} , assuming a dipole field radius of curvature.

If $\gamma_{PFF} > \gamma_C$, then the copious curvature photons will pair-produce, and the observed radiation will be the synchrotron emission of the generated pairs. At low energies, $\epsilon < \epsilon_a/(1+a^2) \ln \Lambda$ in the notation of Paper II, the spectral index is the $-2/3$ of unprocessed synchrotron radiation, while at higher energies, the spectral index is the characteristic $-3/2$.

If $\gamma_{PFF} < \gamma_C$, then the curvature photons will be observed directly. The beam energy loss in this case, for all pulsars examined, is small enough that the characteristic curvature energy remains effectively unchanged. Therefore, the unmodified $-2/3$ spectrum of curvature radiation will be seen, extending from low energies up to $\epsilon_C(\gamma)$. This energy will clearly be lower than the traditional estimate of the cut-off energy of ϵ_a and dependant on the mechanism which sets the PFF.

Figure 3 shows the results of dividing the pulsars into two categories, based on this division. Out of the top 20 brightest expected polar-cap γ -ray pulsars, only two are expected to have the $-2/3$ power law, J0953+0755 and J1932+1059. To illustrate the difference, we plot in Figure 4 the numerically-calculated γ -ray spectrum of J1952+3252, which is expected to have a $-3/2$ spectrum, and J1932+1059. The numerical method used was that described in Paper II, and the results confirm the expectations.

The maximum energies of these spectra depend on whether the beam is radiation-reaction limited or not, not on the minimum energy for pair production, ϵ_a . All photon energies higher than ϵ_a are converted by pair production to photons of lower energy, but ϵ_a steadily increases with altitude as r^3 , eventually surpassing the maximum energy of the raw photon spectrum emitted by the beam particles. At that point, and beyond, the maximum energy of the spectrum is set by the energy of the beam itself.

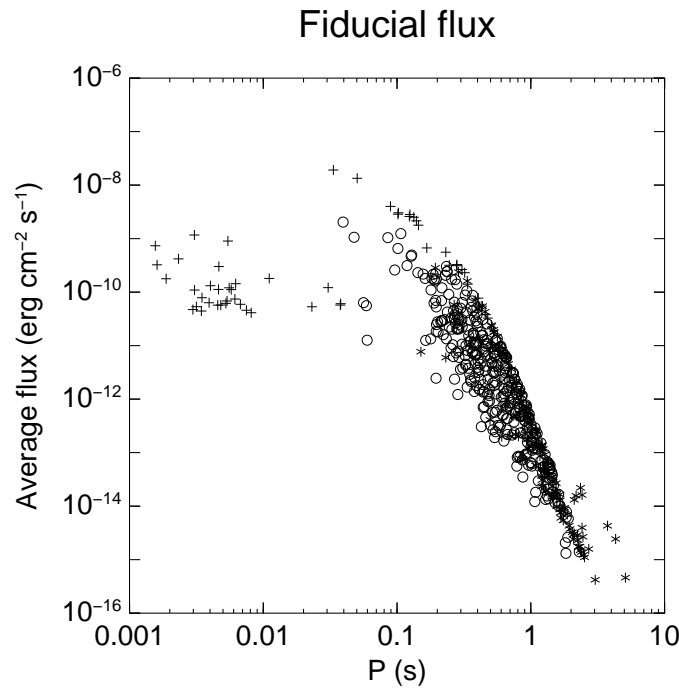


FIG. 1.— γ -ray flux expected from pulsars, as a function of pulse period, if all pulsars are placed at a fiducial distance of 1 kpc.

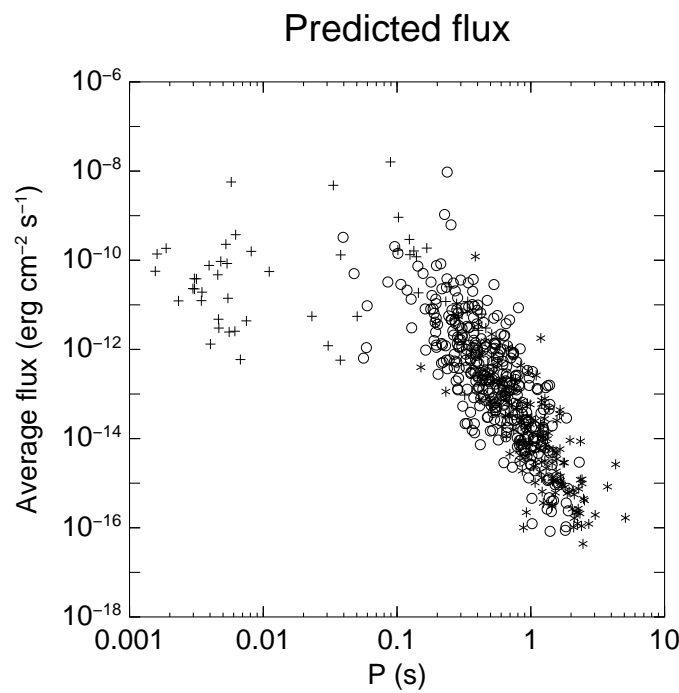


FIG. 2.— γ -ray flux expected from pulsars, as a function of pulse period, given the actual pulsar distances.

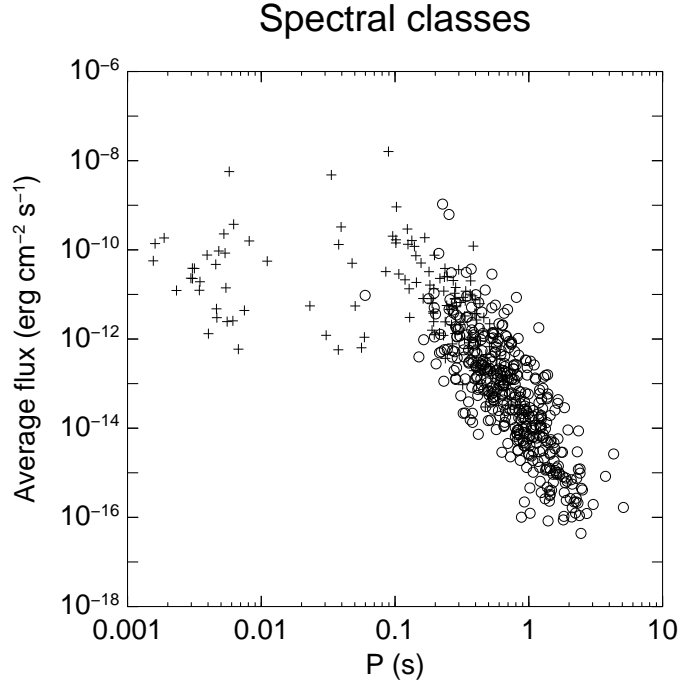


FIG. 3.— Expected observed γ -ray flux vs. pulsar period. Each pulsar has been classified into those where curvature radiation is expected to produce pairs (crosses) and those where it is not (circles). Pulsars where curvature emission produces pairs are expected to have a spectral index of $-3/2$, while those which do not are expected to have an index of $-2/3$.

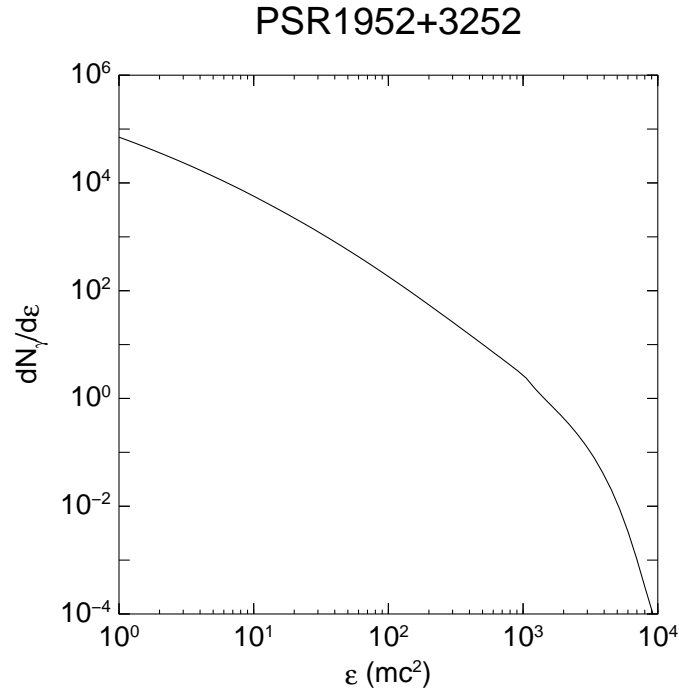


FIG. 4.— Predicted γ -ray spectrum produced by a single primary particle for 1952+3252, illustrating the strong curvature-induced pair production regime, with the resultant $\nu = -3/2$ power-law spectrum. The spectrum is given in units of N/mc^2 .

PSR1932+1059

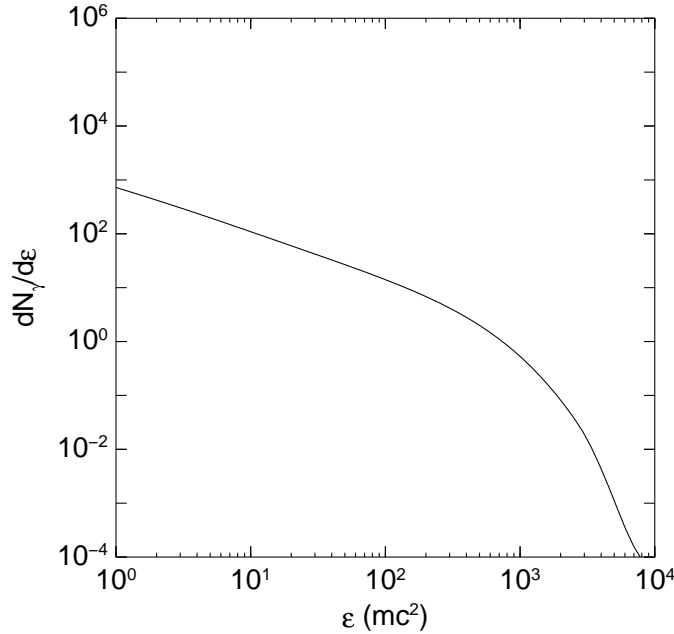


FIG. 5.— Predicted γ -ray spectrum produced by a single primary particle for 1932+1059, illustrating the sparse pair production regime, with the resultant $\nu = -2/3$ power-law. The spectrum is given in units of N/mc^2 .

Since curvature radiation is the strongest emission mechanism for all of the brightest pulsars and all but a small minority of the others, the maximum energy will be the characteristic curvature energy, evaluated at the high-altitude coasting Lorentz factor of the beam. However, the relevant Lorentz factor is slightly different from that calculated in the previous section, equation (6). Since the radius of curvature of the field steadily increases with altitude, the curvature energy of a coasting beam will steadily decrease, as $r^{-1/2}$. The maximum energy observed will then arise from emission from an intermediate regime; high enough that the magnetic field no longer absorbs photons, but low enough that the radius of curvature is still small. In this case, the appropriate limiting Lorentz factor is where the scale height for energy loss is equal to the stellar radius, $\gamma'_{RR} = 3.56 \times 10^7 P^{1/3}$.

If the beam is radiation-reaction limited in this sense, i.e. if $\gamma_{PFF} > \gamma'_{RR}$, then the maximum energy is the curvature energy evaluated at γ'_{RR} , or

$$\epsilon_{max}^{RR} = \epsilon_C(\gamma'_{RR}) = 10.2 P^{1/2} \text{ GeV} \quad (29)$$

where we have evaluated the curvature energy at a radius of $2R_*$.

If the beam is not radiation-reaction limited, then the maximum energy depends on the Lorentz factor of the beam, through

$$\epsilon_{max}^{coast} = \epsilon_C(\gamma_{PFF}) = 3.2 \times 10^{-22} P^{-1/2} \gamma_{PFF}^3 \text{ GeV.} \quad (30)$$

The expected observable fluxes and maximum energies for the 25 brightest pulsars are shown in Table 1.

4. NUMERICAL MODEL

Using the full numerical system described in Section 4 of Paper II, we have run several simulations of these objects. These results confirm our conclusions about the different

regimes of pair production discussed above, with the numerically calculated luminosity remaining within approximately a factor of 3 of the simple analytic model, with the numerical model always lower, due to the effects of pair creation on the tails of the distribution. Over the 25 brightest pulsars, the numerical results are on average of a factor of 2.1 lower than the theoretical results, although the brightest pulsars show more variance.

The calculated pulsar spectra matched expectations, although in several cases a low-intensity high-energy tail due to NRICS was observed, extending up to γ_{PFF} with a power law exponent of roughly -2. In general, this tail contains a negligible portion of the energy, namely the energy predicted by equation (2).

We also ran the numerical model using alternative heating models. We found that, since in the brightest objects curvature emission sets the PFF, the precise temperature model mattered little for the observed objects. Using different models of the stellar temperature only changed the expected luminosity by on the order of 20%. However, for the lower-luminosity ICS-dominated pulsars, the temperature is far more important, as the ICS process relies on the thermal photon bath, potentially allowing future γ -ray observations to discriminate between thermal models.

5. DISCUSSION

In Table 2, we compare the observed flux, the flux by the model of Zhang & Harding (2000), the flux predicted by the semi-numerical model of this paper, and the flux computed by running the full numerical cascade model for each of the observed γ -ray pulsars. The flux predicted for both models was derived from the total luminosity using equation (27).

The model of Zhang & Harding (2000) assumed that $\alpha = 30$, decreasing the expected flux, while invoking a

TABLE 1
BRIGHTEST PULSARS

Pulsar	P (s)	B (Gauss)	PFF mech.	RR limited?	Curv. pairs?	ϵ_{max} (GeV)	Predicted Flux (erg cm $^{-2}$ s $^{-1}$)
J0835-4510	0.089	6.8×10^{12}	Curv	Yes	Yes	3.07	1.6×10^{-8}
J0633+1746	0.237	3.3×10^{12}	NRICS	Yes	Yes	3.73	9.5×10^{-9}
J0437-4715	0.006	1.2×10^9	Curv	Yes	Yes	0.78	5.7×10^{-9}
J0534+2200	0.033	7.6×10^{12}	Curv	Yes	Yes	1.88	4.8×10^{-9}
J1932+1059	0.227	1.0×10^{12}	NRICS	No	No	0.81	1.1×10^{-9}
J1709-4428	0.102	6.3×10^{12}	Curv	Yes	Yes	3.29	9.2×10^{-10}
J0953+0755	0.253	4.9×10^{11}	NRICS	No	No	0.55	6.2×10^{-10}
J1300+1240	0.006	1.7×10^9	Curv	Yes	Yes	0.81	3.7×10^{-10}
J1952+3252	0.040	9.7×10^{11}	NRICS	Yes	Yes	2.04	3.3×10^{-10}
J1048-5832	0.124	7.0×10^{12}	Curv	Yes	Yes	3.61	2.9×10^{-10}
J1012+5307	0.005	5.6×10^8	Curv	Yes	Yes	0.74	2.3×10^{-10}
J2043+2740	0.096	7.0×10^{11}	NRICS	Yes	Yes	3.18	2.0×10^{-10}
J0742-2822	0.167	3.4×10^{12}	Curv	Yes	Yes	4.19	1.9×10^{-10}
J0034-0534	0.002	2.3×10^8	Curv	Yes	Yes	0.44	1.9×10^{-10}
J1826-1334	0.101	5.6×10^{12}	Curv	Yes	Yes	3.27	1.7×10^{-10}
J1803-2137	0.134	8.6×10^{12}	Curv	Yes	Yes	3.75	1.6×10^{-10}
J1730-2304	0.008	7.9×10^8	Curv	Yes	Yes	0.93	1.6×10^{-10}
J0117+5914	0.101	1.6×10^{12}	NRICS	Yes	Yes	3.27	1.4×10^{-10}
J1959+2048	0.002	3.3×10^8	Curv	Yes	Yes	0.41	1.4×10^{-10}
J1801-2451	0.125	8.1×10^{12}	Curv	Yes	Yes	3.63	1.3×10^{-10}

TABLE 2
OBSERVED AND PREDICTED PULSAR FLUXES

Pulsar	B (Gauss)	PFF mech.	ϕ_{obs}^a (erg cm $^{-2}$ s $^{-1}$)	ϕ_{zhang}^b (erg cm $^{-2}$ s $^{-1}$)	ϕ_{pred} (erg cm $^{-2}$ s $^{-1}$)	ϕ_{num} (erg cm $^{-2}$ s $^{-1}$)
J0534+2200	7.6×10^{12}	Curv	1.3×10^{-8}	5.9×10^{-9}	4.8×10^{-9}	1.8×10^{-9}
J0835-4510	6.8×10^{12}	Curv	9.9×10^{-9}	2.3×10^{-8}	1.6×10^{-8}	5.0×10^{-9}
J0633+1746	3.3×10^{12}	NRICS	3.9×10^{-9}	2.6×10^{-8}	9.5×10^{-9}	4.5×10^{-9}
J1709-4428	6.3×10^{12}	Curv	1.3×10^{-9}	1.3×10^{-9}	9.2×10^{-10}	3.0×10^{-10}
J1513-5908	3.1×10^{13}	RICS	8.8×10^{-10}	5.3×10^{-10}	4.0×10^{-13}	2.0×10^{-13}
J1952+3252	9.7×10^{11}	NRICS	4.3×10^{-10}	5.1×10^{-10}	3.3×10^{-10}	1.8×10^{-10}
J1057-5226	2.2×10^{12}	NRICS	2.9×10^{-10}	2.5×10^{-10}	7.6×10^{-11}	5.1×10^{-11}
J1048-5832	7.0×10^{12}	Curv	2.5×10^{-10}	4.2×10^{-10}	2.9×10^{-10}	7.5×10^{-11}

^aThompson, et al. (1999)

^bZhang & Harding (2000)

proposed ICS instability to move the acceleration region off the surface of the star. These two effects roughly cancel, leaving the predictions of their model comparable to those of this model, which effectively uses $\cos \alpha = 1$ and acceleration near the surface. Due to the small numbers of reversed particles, we find no instability in the acceleration zone, especially in the cases where, in the language of this paper, curvature radiation sets the PFF. Hence we find no reason to raise the altitude of the acceleration zone.

The numerically calculated result is substantially smaller than either the semi-numerical result or that of Zhang & Harding (2000), due to two major effects. First, the numerically-calculated PFF is lower than that predicted by the analytic model by approximately 25% on average, which, since these pulsars operate in the low-level quadratic portion of the accelerating potential, reduces the Lorentz factor of the beam to approximately 60% of its analytically calculated value. This occurs because photons on the exponential tail of the curvature spectrum pair produce and create a sufficiently dense plasma to short out the accelerating electric field at lower altitudes than expected in cruder calculations (Arons & Scharlemann 1979).

The second reason is that some of the primary photon energy remains in the generated pairs, rather than being re-radiated. Both the analytic model of this paper and that of Zhang & Harding (2000) assume that *all* of the energy emitted by the primary beam is eventually re-emitted in γ -rays, due to the combination of synchrotron emission from the created pairs and RICS extracting any remaining energy. In the numerical model, however, we calculate the pair spectrum itself and can determine what fraction of the energy in the pairs is re-radiated by RICS.

As a quick approximation to the effects of RICS on the pair spectrum, we assume that all particles with an energy loss length scale equal to or less than the stellar radius re-emit all of their energy as lower-energy γ -rays. The minimum Lorentz factor is the lowest at which thermal photons could be scattered into resonance with the field, $\gamma_{min} = \epsilon_B / \Delta \mu kT = 134.5 B_{12} T_6^{-1} \Delta \mu^{-1}$. The maximum Lorentz factor is the point where the particle's energy loss scale is a stellar radius, $\gamma_{max} = 4.05 \times 10^3 B_{12} T_6^{1/2}$.

With these corrections, we see that the predictions of the polar cap model are low compared to the observations for most of the observed γ -ray pulsars. The difference is large for the Crab, for which the prediction is low by a factor of 10, and for the high-field object 1513-5908, which is low by three orders of magnitude. The other objects are typically low by a factor of three.

The high-field object 1513-5908 clearly deserves further examination. Not only is this magnetic field of this pulsar so large that the applicability of this model is questionable, due to high-field effects as discussed by Harding, et al. (1997), but preliminary studies of the spatial variation of γ -ray emission across the polar cap suggest that the core of this pulsar's beam should be much brighter than the edge field line considered in this model.

The neglect of spatial variation across the polar cap limits the accuracy of these results; simple estimates suggest that including those effects would increase the expected flux by 50%, but more detailed study is required to be more concrete. Physically, the general-relativistic acceleration is strongest at the center of the pulsar, while the field

line radius of curvature is smallest at the edge. Due to the smaller radius of curvature and gentler acceleration, pair production due to ICS processes is far easier at the edges of the polar cap than at the center, while pair production via curvature radiation is more likely on the central field lines. Together, these effects combine to place the pair formation front at a higher altitude in the center of the polar cap and lower near the edges, so that the central field lines are comparatively brighter than the edges.

These effects should help raise the predicted luminosities closer to those observed, bringing them within the expected margins of error for this study. Further work on the variation of the γ -ray emission across the polar cap is certainly required before any firm conclusions can be drawn.

However, the polar cap model gives specific predictions for the beaming which are not consistent with the observations. First, the γ -ray peaks should be in phase with the radio emission, which is not typically the case. Second, for all of the observed pulsars, the curvature emission energy loss, equation (4), predicts that 40–60% of the emitted energy for these pulsars should be emitted within the first 10 km above the surface. This energy would go into a cone of angular width $\theta_{emit} = 2(3/2)^{1/2} \theta_c$ or $\theta_{emit} = 3.5 P^{-1/2}$ degrees. This is far more focused than the observed pulsars, which have double beam profiles spread over rotation phase 0.4, typically. If the observed pulsars were all oriented with the magnetic axis, rotation axis, and line of sight all roughly parallel, such broad profiles could be generated by a polar cap model. Specific modeling of the polar cap model's beaming properties require the angle between the rotation axis and the magnetic axis to be less than 45 degrees and the intrinsic opening angle of the beam to be as large as 30 degrees (Harding & Daugherty 1998). The restriction on obliquity is *a priori* improbable, and is known to cause difficulty with the population statistics of pulsars (Romani 1996), while the large opening angle for the intrinsic emission beam requires adding new features to the basic dynamics of the polar cap model not supported by our calculations.

Given these beaming problems with the polar cap model, the outer gap models of Romani & Yadrioglu (1995); Yadrioglu & Romani (1995); Zhang & Cheng (1997) remain strong contenders for the EGRET pulsars. These models easily produce beam profiles which resemble the data, but are energetically more difficult. For example, recent work by Hirotani & Shibata (2001) addresses the over-abundance in TeV emission, but the emissivity in the GeV range remains an open question.

However, even if the observed γ -ray emission originates in the outer magnetosphere, the flux predicted to arise from the polar cap itself is not so far less than the observed fluxes as to be unobservable in the near future. With the advent of the new γ -ray instruments, the threshold of sensitivity should be low enough that the polar cap γ -rays can be observed. Detection of these gamma rays, seen when looking down the barrel of the radio gun, and comparison of their emission phase and profile with the radio counterpart, would be a firm test of the long established, but not directly tested, theory of polar cap pair creation which underlies 30 years of theorizing about the origin of pulsar radio emission.

6. CONCLUSION

The primary conclusion of this paper is that the currently observed γ -rays pulsars are *not* representative of the bulk of pulsars. Currently, only the brightest γ -ray pulsars are observed; these pulsars are selected to be those where curvature radiation operates efficiently, which is not true of pulsars in general.

Most pulsars have a beam energy controlled by nonresonant inverse Compton scattering (NRICS), rather than curvature emission, and will emit significantly fewer γ -rays. Locating examples of these objects will be a challenge to the new generation of γ -ray telescopes. The fainter the objects which can be seen, the stronger the differences should be between the NRICS cascades and the predictions of the curvature-based PFF models.

In these fainter objects, the separation of the mechanism producing the PFF (and thus shorting out the accelerating potential) from the mechanism producing most of the observable γ -rays should reveal itself through differing spectral indices. Due to the effects of inverse Compton scattering, there should exist two classes of observed γ -

ray emission, one a raw curvature spectrum characterized by a spectral index of $-2/3$, and the other a saturated synchrotron response with a spectral index of $-3/2$.

For the currently observed γ -ray pulsars, the predicted fluxes are consistently low, although, due to the neglect of spatial variation across the polar cap, they are within the accuracy of this study. The beaming issues with the polar-cap model remain; for this reason, the outer-gap models are still strong contenders for the observed pulsars, despite the energetic problems of those models. Even if the currently observed emission is from an outer gap, improved γ -ray sensitivity should reveal the signal of the polar caps, which is at worst only a factor of 5 below the observed fluxes.

Further observations should also reveal the differences in the luminosity classes of polar cap γ -rays, according to which mechanism which creates the PFF, and the differences between the two spectral regimes, providing a straightforward test of this model.

The author would like to thank the referee for several helpful suggestions.

REFERENCES

Arons, J., & Scharlemann, E.T., 1979, ApJ, 231, 854
 Daugherty, J. K., & Harding, A. K. 1982, ApJ, 252, 337
 Dermer, C.D., 1990, ApJ, 360, 197
 Harding, A. K., Baring, M. G., & Gonthier, P. L. 1997, ApJ, 476, 246
 Harding, A. K., & Muslimov, A. G. 1998, ApJ, 508, 328
 Harding, A. K., & Daugherty, J. K. 1998, Advances in Space Research, 21, 251
 Hibschman, J.A., & Arons, J. 2001, ApJ, 546, 382 (Paper I)
 Hibschman, J.A., & Arons, J. 2001, ApJ, in press (Paper II)
 Hirotani, K., & Shibata, S. 2001, MNRAS, 325, 1228
 Jackson, J.D. 1975, Classical Electrodynamics (2d ed.; New York: John Wiley & Sons, Inc.)
 Luo, Q. 1996, ApJ, 468, 338
 Muslimov, A. G., & Tsygan, A. I. 1992, MNRAS, 255, 61
 Muslimov, A. G., & Harding, A. K. 1997, ApJ, 485, 735
 Romani, R.W., & Yadrioglu, I.-A., 1995, ApJ, 438, 314
 Romani, R.W. 1996 in ASP Conf. Ser. 105, Pulsars: Problems and Progress: IAU Colloq. 160, ed. S. Johnston, M.A. Walker, & M. Bailes (San Francisco: ASP), 331
 Sturner, S. J., Dermer, C. D., & Michel, F. C. 1995, ApJ, 445, 736
 Sturner, S. J. 1995, ApJ, 446, 292
 Thompson, D.J., et al. 1997, in AIP Conf. Proc. 410, Proc. Fourth Compton Symp., ed. C. Dermer, M.S. Strickman, & J.D. Kurfess (New York: AIP), 39
 Thompson, D.J., et al. 1999, ApJ, 516, 297
 Ulmer, M.P. 1994, ApJS, 90, 789
 Yadrioglu, I.-A., & Romani, R.W., 1995, ApJ, 449, 211
 Zhang, L., & Cheng, K.S., 1997, ApJ, 487, 370
 Zhang, B., & Harding, A.K., 2000, ApJ, 532, 1150